Desalination and Water Treatment
www.deswater.com

doi: 10.5004/dwt.2018.23229

136 (2018) 356–368
December

Comparative performance of aerobic and anaerobic environments on simultaneous removal of Cd^{2+} and Mn^{2+} by Fe–electrocoagulation

Longqian Xu[a], Xiaojun Xu[a], Guangzhu Cao[b,*], Shuli Liu[a], Zhengyang Duan[a]

[a]*Faculty of Environmental Science and Engineering, Kunming University of Science and Technology, Kunming 650500, China, emails: xulq1993@163.com (L.Q. Xu), xuxiaojun88@sina.com (X.J. Xu), 1203293826@qq.com (S.L. Liu), zyduan1990@sina.com (Z.Y. Duan)*

[b]*Faculty of Land Resource Engineering, Kunming University of Science and Technology, 650500 Kunming, China, Tel. +86 13518715129; email: cgzhu@163.com*

Received 31 January 2018; Accepted 30 September 2018

ABSTRACT

In the this work, the performance of Fe–electrocoagulation in anaerobic (ANA) and aerobic (AER) environments for simultaneous removal of Cd^{2+} and Mn^{2+} from synthetic wastewater were investigated. Detailed experiments were carried out to evaluate the effects of oxidants and reductants, initial pH (pH_i), current density (j), nature of the anions, and initial concentration ($[anions]_0$) on electrocoagulation performance. The results showed that ANA process was superior to AER process due to the formation of high proportion of Fe(II)/Fe(III) hydroxide species (green rust). These results were supported by X-ray photoelectron spectroscopy analysis. A high current density favored the heavy metal removal, especially in the ANA process and an R_{Cd} of 95.21% and an R_{Mn} of 93.83% were obtained at a current density of 100 A/m^2. A significant difference was also observed between chloride and sulfate for the heavy metal removal; chloride was more suitable for Mn^{2+} removal than sulfate but the opposite was true for Cd^{2+} when the initial anion concentration was 50 mmol/L. However, excess concentrations of chloride and sulfate had an adverse influence on the Cd^{2+} and Mn^{2+} removal in the AER and ANA processes, although the increase in Cl^- (from 10 to 50 mmol/L) and SO_4^{2-} (from 10 to 30 mmol/L) contributed to the removal of Cd^{2+}. Finally, kinetic isotherm and thermodynamic studies were conducted to illustrate the removal mechanisms.

Keywords: Electrocoagulation; Aerobic; Anaerobic; Anions; Heavy metal

1. Introduction

The presence of cadmium (Cd^{2+}) and manganese (Mn^{2+}) in various industrial effluents, such as the smelting, mining, and electroplating industries, has raised serious environmental concern due to the high content, biotoxicity, and carcinogenicity of these heavy metals [1–7]. Particularly, Cd^{2+} and Mn^{2+} are highly water soluble and non–biodegradable in natural ecosystems and concentrations of less than 0.003 and 0.5 mg/L (WHO, 2011), respectively, in drinking water are essential to human health [8–10]. Over the last decades, many techniques, including chemical coagulation, adsorption, ion exchange, reverse osmosis, and membrane filtration (nanofiltration [NF] and ultrafiltration [UF]) have been widely employed in heavy metal wastewater treatment [11–15]. However, these methods all possess shortcomings, such as excessive cost, serious secondary pollution, long run times, and complex processes.

Unlike the above-mentioned methods, electrocoagulation (EC) is considered an alternative and green technique for various kinds of wastewater treatment due to the advantages of high removal efficiency, no chemical requirements, use of simple devices, lack of secondary pollution, etc. [16–18]. During the EC process, large amounts of cations (Fe^{2+} or Al^{3+})

* Corresponding author.

are produced in situ by the anode and are subsequently converted into monomeric and polymeric hydroxide species [19–22], such as $Fe(OH)^+$, $Fe(OH)_3^-$, $Fe_2(OH)_2^{4+}$, $Al(OH)^{2+}$, $Al_2(OH)_2^{4+}$, $Al_7(OH)_{17}^{4+}$, and $Al_{13}(OH)_{34}^{5+}$, by further spontaneous hydrolysis. The main reactions at different pH are shown in Table 1 [23,24].

In the traditional iron electrocoagulation (Fe–EC), two kinds of cations are produced by the sacrificial anode, namely ferrous ions (Fe^{2+}) and ferric ions (Fe^{3+}) and the types of Fe are influenced by the solution pH as shown in Table 1 [25]. The subsequently generated Fe(II) and Fe(III) hydroxide species have the following similarities and differences: (1) among the two cations, Fe^{2+} is directly generated by the anode by electrochemical oxidation. However, Fe^{2+} ions and Fe(II) hydroxides are unstable and highly sensitive to oxidizing agents (dissolved oxygen and chlorine) and can quickly convert into Fe^{3+} and Fe(III) species, especially in the presence of chloride [21,26,27]. (2) Fe^{2+} and Fe^{3+} cations will eventually hydrolyze into hydroxide flocs, which have strong adsorption capacity for most heavy metals. (3) In general conditions, Fe(II) and Fe(III) species in the EC process are presented in the form of complicated hydroxides, various kinds of productions such as goethite [28,29], magnetite [25,30], lepidocrocite [30,31], hematite [32–34], ferrihydrite [35,36], and green rust [30,37,38] can be produced. Although magnetite and green rust consist of Fe(II) and Fe(III) cations in a layered double hydroxide (LDH) structure, the intermediate green rust plays an important role in EC process for contaminants removal [25]. In previous researches [17,30,37,39], the removal of chromium and arsenic is dominated by the existing form of Fe(II) and Fe(III) in wastewater, few studies have focused on the comprehensive performance of LDHs flocs and tried to control its generation by creating aerobic and anaerobic conditions. Therefore, the performance of the Fe(II)/Fe(III) LDHs species with regard to the removal of heavy metals should be investigated.

The primary objective of this study is to investigate the EC performance of anaerobic and aerobic environments on the removal efficiencies of Cd^{2+} (R_{Cd}) and Mn^{2+} (R_{Mn}) from wastewater. (Hereafter aerobic and anaerobic will be abbreviated as ANA and AER, respectively). The existing forms of Fe(II) and Fe(III) hydroxide species are determined under different aerobic and anaerobic conditions, respectively. The removal of Cd^{2+} and Mn^{2+} using under different EC parameters was evaluated using X-ray photoelectron spectroscopy (XPS) analysis. Moreover, the effects of current density (j), initial pH (pH_i), nature of the anions and initial concentration ($[anions]_0$) on the removal of Cd^{2+} and Mn^{2+} were also investigated. Finally, kinetic isotherm and thermodynamic studies were conducted to illustrate the removal mechanisms.

2. Materials

2.1. Synthetic wastewater samples

The stock solutions of Cd^{2+} and Mn^{2+} (both 1,000 mg/L) were prepared by dissolving cadmium chloride ($CdCl_2{\cdot}5/2H_2O$), cadmium sulfate ($CdSO_4{\cdot}8/3H_2O$), manganese chloride ($MnCl_2$), and manganese sulfate ($MnSO_4{\cdot}H_2O$) in deionized water. Na_2SO_4 and/or NaCl salts were added as supporting electrolytes. In addition, the aerobic and anaerobic conditions of the solutions were controlled by adding the appropriate amounts of Na_2SO_3 and H_2O_2, respectively. The pH_i was adjusted to the desired value by adding diluted NaOH (1 M), HCl (1 M), and/or H_2SO_4 (1 M) solutions. All chemicals involved were of analytical grade and were purchased from Sinopharm Chemical Reagent Co., Ltd., China.

2.2. EC setup

Rectangular batch EC cells fabricated from Plexiglas (Nanchang inte Industrial Co., Ltd., China) were constructed to compare the EC performance of AER and ANA

Table 1
Reactions of Fe–electrocoagulation at different solution pH (pH 2, 7 and 12)

Type	Reactions in different solution pH							
	pH 2		pH 7				pH 12	
Anode	$Fe_{(s)} \rightarrow Fe^{2+}_{(aq)} + 2e^-$		$Fe_{(s)} \rightarrow Fe^{2+}_{(aq)} + 2e^-$	$E^0 = +0.447$ V	(5)		$Fe_{(s)} \rightarrow Fe^{3+}_{(aq)} + 3e^-$	
	$E^0 = +0.447$ V	(1)	$Fe^{2+}_{(aq)} \rightarrow Fe^{3+}_{(aq)} + e^-$	$E^0 = -0.771$ V	(6)		$E^0 = +0.037$ V	(12)
			$Fe_{(s)} \rightarrow Fe^{3+}_{(aq)} + 3e^-$	$E^0 = +0.037$ V	(7)			
Cathode	$4H^+_{(aq)} + 4e^- \rightarrow 2H_{2(g)}$		$2H_2O_{(l)} + 2e^- \rightarrow H_{2(g)} + 2OH^-_{(aq)}$				$2H_2O_{(l)} + 2e^- \rightarrow H_{2(g)} + 2OH^-_{(aq)}$	
	$E^0 = 0.000$ V	(2)	$E^0 = -0.828$ V		(8)		$E^0 = -0.828$ V	(13)
Solution	$Fe^{2+}_{(aq)} + 2OH^-_{(aq)} \rightarrow Fe(OH)_{2(s)}$	(3)	$Fe^{2+}_{(aq)} + 2OH^-_{(aq)} \rightarrow Fe(OH)_{2(s)}$		(9)		$Fe^{3+}_{(aq)} + 3OH^-_{(aq)} \rightarrow Fe(OH)_{3(s)}$	(14)
			$Fe^{3+}_{(aq)} + 3OH^-_{(aq)} \rightarrow Fe(OH)_{3(s)}$		(10)			
Total	$2Fe_{(s)} + 6H_2O_{(l)} \rightarrow 2Fe(OH)_{2(s)} + O_{2(g)} + 4H_{2(g)}$	(4)	$3Fe_{(s)} + 8H_2O_{(l)} \rightarrow Fe(OH)_{2(s)} + 2Fe(OH)_{3(s)} + 4H_{2(g)}$		(11)		$2Fe_{(s)} + 6H_2O_{(l)} \rightarrow 2Fe(OH)_{3(s)} + 3H_{2(g)}$	(15)

environments on the simultaneous removal of Cd^{2+} and Mn^{2+}. The schematic diagram and dimensions of EC reactor are shown in Fig. 1. In each experiment, wastewater samples of a fixed volume (500 mL) were poured into the reactors. A pair of iron plates (purity > 99.0%) with an effective surface area of 50 cm^2 were installed vertically in monopolar mode and connected to a DC power supply (SMD–60P, China). The separation distance of iron plates was fixed at 2.0 cm. During EC process, water samples were agitated using a magnetic stirrer at a rotational speed of 150 rpm and all experiments were conducted at a steady room temperature of 298 ± 0.5 K.

2.3. Analytical procedure

In the preparation phase, iron plates were cleaned using sandpaper, diluted hydrochloric acid solution, ultrapure water, and vacuum drying. The binary metal working solutions of Cd^{2+} (50 mg/L) and Mn^{2+} (60 mg/L) were prepared by the corresponding stock solutions described above. The influence of ANA and AER conditions were evaluated based on various operating parameters, such as the oxidants and reductants, initial pH (pH_i), the current density (j), and the initial chloride $[Cl^-]_0$ and sulfate $[SO_4^{2-}]_0$ concentrations. During the EC process, water samples of 20 mL were periodically taken and filtered (0.45 μm filter membrane) to determine the residual concentrations of Cd^{2+} and Mn^{2+} using an atomic absorption spectrophotometer (TAS–990, China). In the meantime, well-mixed solutions containing masses of small floc particles were immediately sampled from the EC reactors and the zeta potentials of the Fe hydroxide flocs were directly measured using a micro–electrophoresis apparatus (HS94H, China). The Fe(II) and Fe(III) concentrations were determined by o–phenanthroline spectrophotography using an ultraviolet–visible (UV–vis) spectrophotometer (L5S, China). Finally, the precipitated samples were analyzed by XPS (ESCALAB 250XI, United States). The removal efficiencies of the Cd^{2+} (R_{Cd}) and Mn^{2+} (R_{Mn}) were calculated using the following formula:

$$R_e(\%) = \frac{C_0 - C_t}{C_0} \times 100 \quad (1)$$

where C_0 and C_t are the initial (before EC) and final (after t_{EC} [min]) concentration, mg/L, respectively.

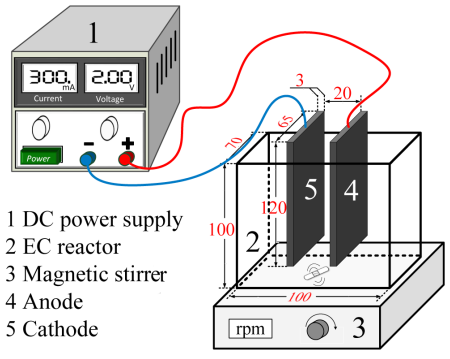

Fig. 1. Schematic diagram of the EC system.

3. Results and discussion

3.1. Effect of oxidants and reductants

The existing states of the iron species are dominated by the solution pH, dissolved oxygen (DO) concentration, as well as chemical agents of the solution. According to previous references [28,40], Fe(II) species are easily transformed into Fe(III) when there are enough oxidant agents in solution. In order to investigate, the performance of Fe hydroxide species, AER and ANA environments were created using hydrogen peroxide (H_2O_2) and sodium sulfite (Na_2SO_3) according to Eqs. (2) and (3). The effective dosage of H_2O_2 and Na_2SO_3 was 5 mmol/L. In addition, control groups were used with the same operating parameters, including 'CG' (control group), 'ANA–SO_4^{2-}', and 'CG–SO_4^{2-}'. The initial solution pH of all experiments was adjusted to 8.20 ± 0.10 because the excess Na_2SO_3 maintains the solution pH at 8.2 due to the hydrolysis reaction as shown in Eqs. (4) and (5).

$$2SO_{3(aq)}^{2-} + O_{2(g)} \rightarrow 2SO_{4(aq)}^{2-} \quad (2)$$

$$2H_2O_{2(l)} \rightarrow 2H_2O_{(l)} + O_{2(g)} \uparrow \quad (3)$$

$$SO_{3(aq)}^{2-} + H_2O_{(l)} \leftrightarrow HSO_{3(aq)}^{-} + OH_{(aq)}^{-} \quad (4)$$

$$HSO_{3(aq)}^{-} + H_2O_{(l)} \leftrightarrow H_2SO_{3(aq)} + OH_{(aq)}^{-} \quad (5)$$

The changes in the R_{Cd} and R_{Mn} over the reaction time under different ANA and AER conditions are shown in Fig. 2. The results indicated that the anoxic environments have a more positive effect on both the Cd^{2+} and Mn^{2+} removal than oxygen-enriched environments, although passivation was achieved in both samples as a result of the current efficiency (Φ) of the sacrificial anode as shown in Fig. 2(d). The addition of Na_2SO_3 reduced the dissolved oxygen in solution to maintain a relatively anoxic environment of the Fe–EC system. Consequently, the equilibrium of Fe(II) to Fe(III) was slowed down by controlling the reaction rate with oxygen. In contrast, the addition of the oxidant agents promoted the transformation efficiency of Fe(II) into Fe(III). In addition, the removal efficiency under different kinds of oxidation and reduction conditions from high to low were ANA, CG, and AER. Fig. 2(a) shows that the corresponding R_{Cd} were 85.93%, 77.1%, and 45.1% after 40 min of treatment and the R_{Mn} were 65.1%, 54.75%, and 33.1%, respectively, (Fig. 2(b)). The addition of SO_4^{2-} favored the removal of Cd^{2+} but inhibited the removal of Mn^{2+}, indicating that SO_3^{2-} is more suitable for heavy metal removal.

The performance of the ANA was better than that of the AER and was attributed to the adsorption capacity of the flocs due to the presence of SO_3^{2-}. Fig. 2(c) indicates that the zeta potentials of the hydroxide flocs for CG, AER, and AER–SO_4^{2-} remained positive (after 10 min), whereas that of the flocs generated in the presence of either SO_3^{2-} or SO_4^{2-} is below 0 mV. This result is consistent with the results of many previous studies that negatively charged flocs contribute to the removal of positively charged metal cations to form

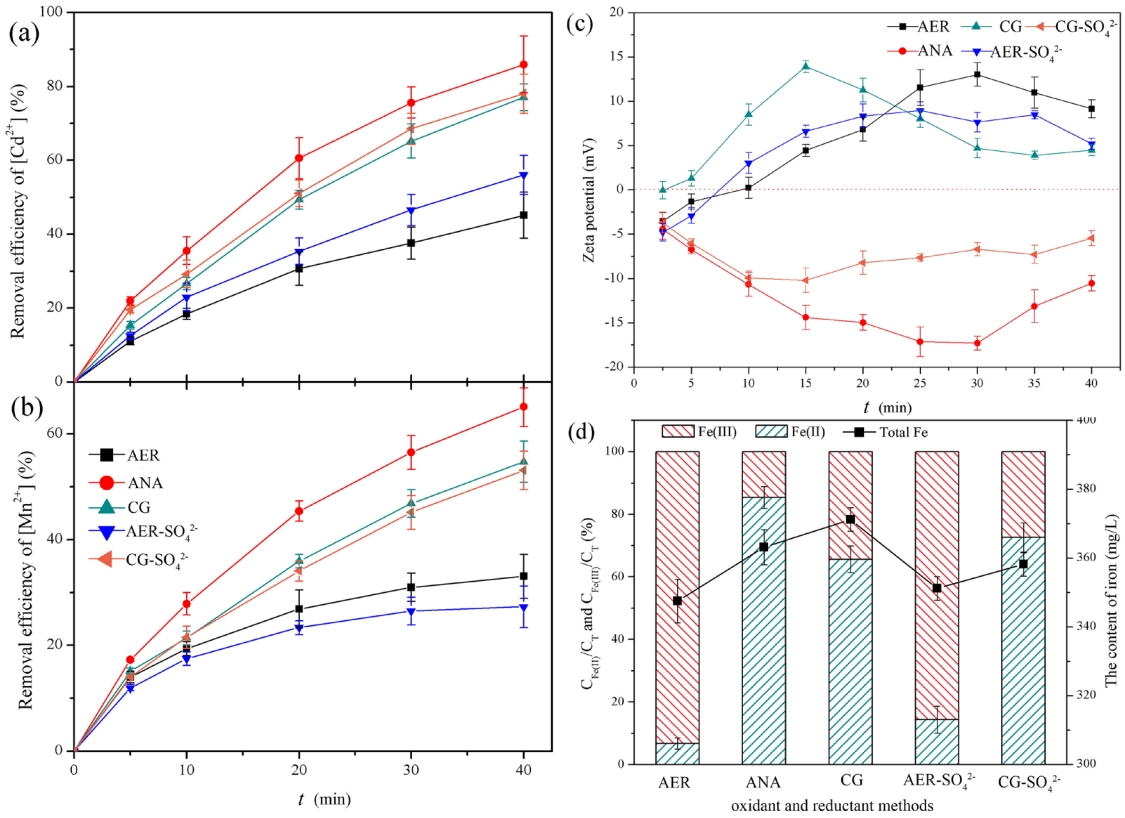

Fig. 2. Effect of oxidants and reductants on (a) Cd^{2+} removal, (b) Mn^{2+} removal, (c) zeta potential of flocs, and (d) content of Fe(II), Fe(III), and total Fe (pH_i = 8.2, j = 60 A/m^2 and $[Cl^-]_0$ = 20 mmol/L).

stable flocs and precipitates [41,42]. This observation also reflects the stronger electrostatic absorbability of fresh flocs, which have a larger specific surface area and flocculation efficiency, which were generated in the sulfite and sulfate solutions. Furthermore, the significant advantages of SO_3^{2-} for the removal of Cd^{2+} and Mn^{2+} can also be ascribed to the green rust, a high ratio of Fe(II)/Fe(III) hydroxides, generated during the ANA process. A similar result was observed by Cao et al. [25] who reported that the content of Fe(II) in the precipitate was higher than that of Fe(III) during the Fe–EC process when Mn^{2+} was present. Moreover, the reason that the current efficiency (Φ) of the different methods did not achieve the theoretical value (Faraday's law, 420 mg/L) might be attributed to the passivation of the anode electrode.

3.2. XPS characterization

XPS was used to analyze the precipitation produced during the AER and ANA processes. As shown in the spectra in Fig. 3, the precipitate formed in the presence of ANA exhibits stronger intensities of Mn2p and Cd3d and a higher percentage of elements (At%) than the precipitate from the AER process, which is consistent with the removal efficiency of Cd^{2+} and Mn^{2+} that is shown in Figs. 2(a) and (b). Moreover, for the ANA process, only the peak of S2p (168.5 eV) is observed, indicating that the Na_2SO_3 has transformed into Na_2SO_4. It can be inferred that the constitution and characteristics of the Fe hydroxides were changed as a result of the addition of SO_3^{2-}.

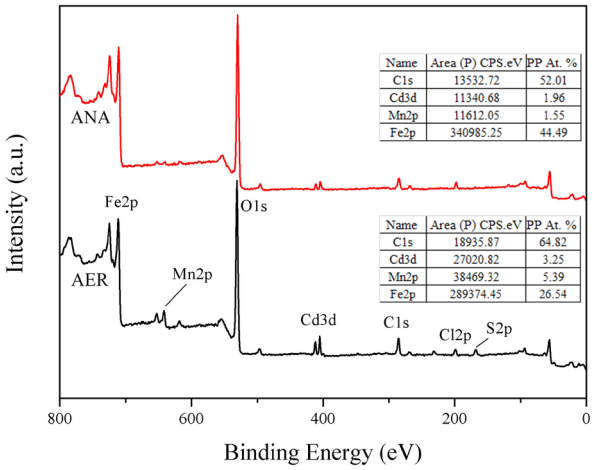

Fig. 3. XPS analysis of EC flocs under AER and ANA conditions.

In the traditional process (open EC system), the Fe(II) and Fe(III) species coexist and share the responsibility for pollutant removal [43]. This is contributed to one of the following reasons as shown in Fig. 4(a): (i) according to Henry's law, the dissolved oxygen in the raw water originates from the dissolution of oxygen. (ii) Oxygen is also created by the electrolysis of water. (iii) Chloride (NaCl), which is the most widely used electrolyte, at the surface of the anode can also be converted to Cl_2 by electrochemical oxidation at high voltage of anode. For instance, the Cl^- ions in solution can be directly oxidized by

anode reaction to ClO_2 (E^0 = 1.599 V) [44]. (iv) Subsequently, the production of various chlorinated by-products, such as hypochlorous acid (HClO), hypochlorite (ClO^-), chlorine dioxide (ClO_2), and chlorite (ClO_2^-) accelerate the formation of Fe(III) species. The types of species and their distribution in solution are determined by the pH. Acidic solutions were reported to favor the formation of chlorine dioxide, whereas alkaline conditions tend to produce chlorate. (v) The yield of most of these perchlorates such as ClO_2^-, ClO_3^-, and ClO_4^- (Eqs. (21)–(27)) generated in EC is minimized because of the low anode potential [44]. (vi) The generated ClO^- ions act as the main oxidizing agent which can interact with Fe^{2+}/Fe(II), and thus promoted the generation of Fe(III) coagulation species. (vii) The floating sludge of Fe(II) on the surface of the solution, which is a result of the electroflotation of H_2, is more easily oxidized into Fe(III) by oxygen form the air than sludge below the water surface. Hence, the generation of Fe(III) is unavoidable, especially if there is an excess amount of chlorine salts in the wastewater. However, the Fe(III) hydroxides likely accounted for a small portion of total iron species based on the color of the solution. The vast majority of iron species existed in the form of ferrous hydroxides/hydrous hydroxides and free Fe^{2+} ions as shown in Fig. 4(b). The color of the high proportion of Fe(III)/Fe(II) flocs generated by the AER process was reddish-brown, whereas the green rust (low percentage of Fe(II)) had a light–green color.

Side reactions of chloride:

$$2Cl^-_{(aq)} \rightarrow Cl_{2(g)} + 2e^- \qquad E^0 = +1.447\ V \tag{6}$$

$$Cl_{2(g)} + H_2O_{(l)} \rightarrow HClO_{(aq)} + H^+_{(aq)} + Cl^-_{(aq)} \quad E^0 = +1.579\ V \tag{7}$$

$$HClO_{(aq)} \rightarrow H^+_{(aq)} + ClO^-_{(aq)} \tag{8}$$

$$Cl^-_{(aq)} + 2OH^-_{(aq)} \rightarrow ClO^-_{(aq)} + H_2O_{(l)} + 2e^- \quad E^0 = +0.89\ V \tag{9}$$

$$ClO^-_{(aq)} + 2OH^-_{(aq)} \rightarrow ClO^-_{2(aq)} + H_2O_{(l)} + 2e^- \quad E^0 = +0.67\ V \tag{10}$$

$$ClO^-_{2(aq)} + 2OH^-_{(aq)} \rightarrow ClO^-_{3(aq)} + H_2O_{(l)} + 2e^- \quad E^0 = +0.33\ V \tag{11}$$

$$ClO^-_{3(aq)} + 2OH^-_{(aq)} \rightarrow ClO^-_{4(aq)} + H_2O_{(l)} + 2e^- \quad E^0 = +0.35\ V \tag{12}$$

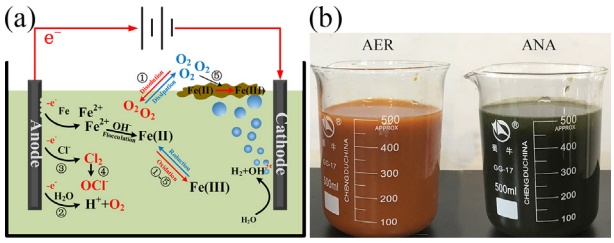

Fig. 4. Oxidizing process (a) and the appearance of flocs (b) in AER and ANA process.

In this study, the presence of the Na_2SO_3 and H_2O_2 intensified the transformation from Fe(II) to Fe(III) by eliminating and releasing O_2, respectively. This process can be divided into two parts: direct oxidation and indirect oxidation [45]. In the ANA system, the addition of Na_2SO_3 created a relatively oxygen-free environment because of the consumption of DO, leading to Fe(II) hydroxides existed in solution provisionally, with the oxidation of Fe(II) into Fe(III) by O_2 and Cl production by anodic reactions, the form of GR promotes the removal of Cd^{2+} and Mn^{2+} because of the high adsorption capacity of Fe(II)/Fe(III) LDHs. The existence of SO_4^{2-} promoted heavy metals removal because of divalent SO_4^{2-} ions has stronger electric neutralization than monovalent Cl^- ion. Furthermore, SO_4^{2-} can also promote the flocculation and settling efficiency of GR flocs, larger size of GR flocs was also observed than single Cl^- solution. Therefore, Cd^{2+} and Mn^{2+} were removed by adsorption and co-precipitation of GR hydroxides flocs. In addition, some of Fe^{2+} in the GR might be replaced by divalent Cd^{2+} or Mn^{2+} ions to form unstable [Fe(II)/Cd(II), Fe(III)] LDHs.

3.3. Effect of initial pH

Fig. 5 shows the final removal efficiency of Cd^{2+} and Mn^{2+} under AER and ANA after 40 min EC. The results indicated that higher removal efficiencies of Cd^{2+} and Mn^{2+} significantly increased with increasing initial pH from 3.2 to 9.5, suggesting that greater amount of Fe hydroxide coagulations were produced and thus promoted the removal of heavy metals. There was little difference of the removal efficiency of Mn^{2+} under AER and ANA conditions when pH_i was 3.2, further increasing pH_i lead to obvious difference that ANA condition positively affect Mn^{2+} removal. ANA also favored Cd^{2+} removal and the removal efficiency reached 96.2%. The increase of the removal of heavy metals under pH_i 9.5 were caused by the increase of solution pH (alkaline solution) which promoted the solubility constants (*Ksp*) for $Cd(OH)_2$ and $Mn(OH)_2$ at 298 K are $10^{-14.3}$ and $10^{-12.7}$, respectively [1,2]. Moreover, the color of the Fe flocs generated in ANA conditions were also dark green at pH 3.2 and 9.5, whereas the

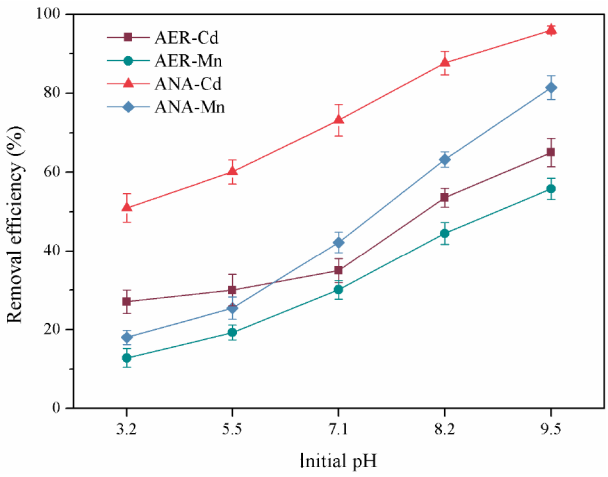

Fig. 5. Effect of initial pH on Cd^{2+} and Mn^{2+} removal efficiency under AER and ANA conditions after 40 min EC (j = 60 A/m² and $[Cl^-]_0$ = 20 mmol/L).

flocs of pH_i 3.2 become reddish-brown faster than that of pH_i 9.5. it can be explained by improving the oxidation efficiency under acid conditions [23].

3.4. Effect of current density

In the EC process, the current density is the most crucial operating parameter because it determines the production of iron coagulation, the generation rate of H_2 bubbles, and the size of the flocs [17,46]. On the other hand, both of the consumption of electric energy and the dissolution of Fe electrode are directly proportional to the applied current according to Eqs. (28) and (29) (Faraday's law). In this study, the AER and ANA experiments were carried out at pH_i = 8.2 and $[Cl^-]_0$ = 20 mmol/L to evaluate the effect of the current densities (j = 20–100 A/m^2) on the Cd^{2+} and Mn^{2+} removal. The removal efficiencies of Cd^{2+} and Mn^{2+} vs. the reaction time and current density for the AER and ANA are shown in Fig. 6.

$$E_{\text{theo}} = \frac{U \cdot I \cdot \text{t}}{V} \tag{13}$$

$$C_{\text{theo}} = \frac{I \cdot t \cdot M}{Z \cdot F \cdot V} \tag{14}$$

here E_{theo} and C_{theo}, respectively, are the theoretical energy consumption (kWh/m^3) and amount of Fe^{2+} ions released (g/L); U and I, respectively, are the voltage (V) and current (A) applied, t is the reaction time (s), M is the molecular weight (g/mol), Z is the number of electrons transferred, Z_{Fe} = 2; F is Faraday's constant, (96,485.34 C/mol), and V is the volume of treated effluent (L).

Figs. 6(a)–(d) show that the increase in j from 20 to 100 A/m^2 led to an increase in the removal efficiency of both Cd^{2+} and Mn^{2+} in the AER and ANA environments. The maximum removal efficiencies of 59.34%, 67.97%, 80.4%, 88.61%, and 95.21% for Cd^{2+} and 35%, 44%, 56.75%, 78.8%, and 93.83% for Mn^{2+} were obtained at the j of 20, 40, 60, 80, and 100 A/m^2, respectively. As reported in a previous reference [46], a higher current density contributed to the release of Fe^{2+} and OH^- directly from the anode and cathode, respectively. Hence, the accumulated Fe(II)/Fe(III) hydroxides adequately removed the heavy metals from the aqueous phase by adsorption or co-precipitation.

However, there are some differences between Cd^{2+} and Mn^{2+} in AER and ANA processes. It can be observed from Figs. 6(a) and (c) that half of the Cd^{2+} is removed in ANA conditions, even at a low current density (59.34% at 20 A/m^2) but only 13.65% of the Cd^{2+} is removed in AER conditions. As j increases, the removal efficiency of Cd^{2+} in AER process increases at a larger rate than in ANA process. The increment of more than 50% is observed when j increases to 100 A/m^2, whereas the removal efficiency of Mn^{2+} in ANA conditions improved from 35% to 93.83% but only from 14.67% to 42.33% in AER conditions (Figs. 6(b) and (d)). Hence, the anaerobic environment and a high current density were more conducive to the removal of Cd^{2+} and Mn^{2+}.

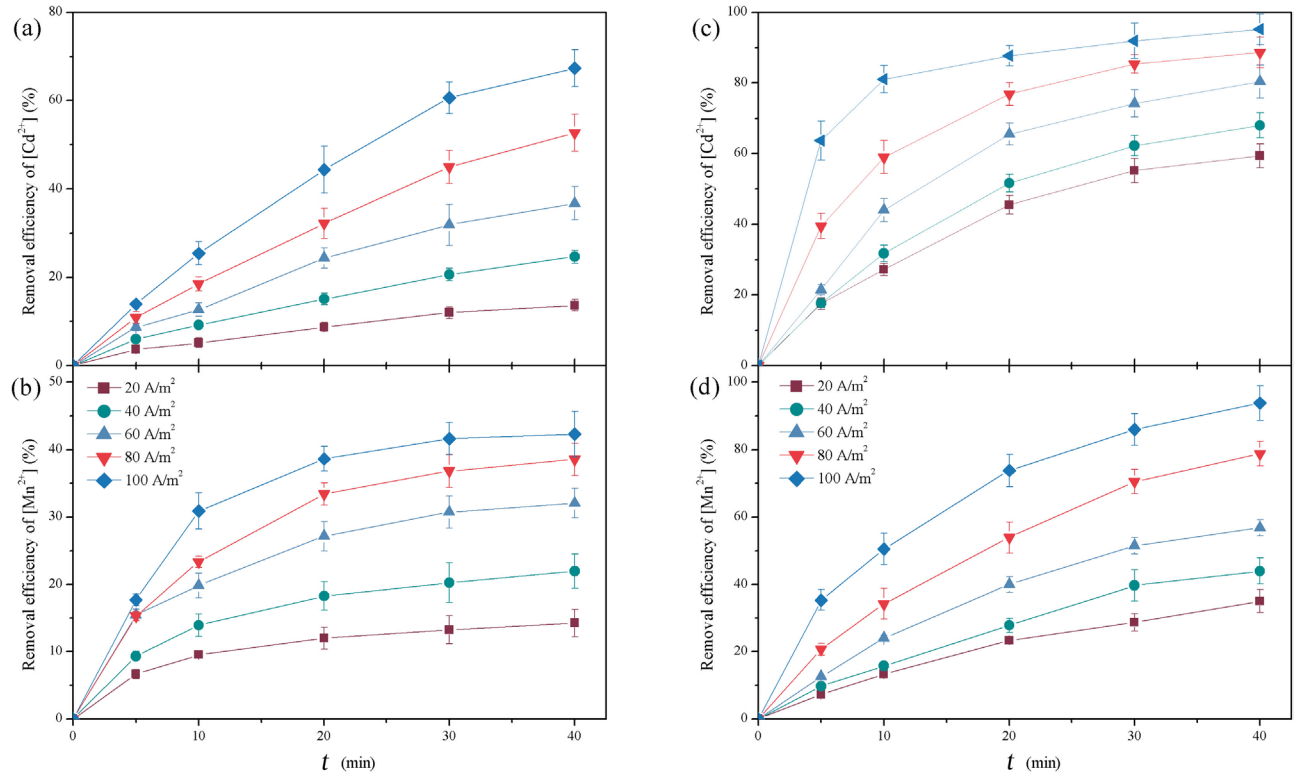

Fig. 6. Effect of current density on (a) Cd^{2+} and (b) Mn^{2+} removal efficiency in AER process and (c) Cd^{2+} and (d) Mn^{2+} removal efficiency in ANA process (pH_i = 8.2 and $[Cl^-]_0$ = 20 mmol/L).

3.5. Effect of anions nature

Generally, industrial wastewaters are rich in Cl^- and SO_4^{2-} and the concentration of these anions is in the range of 5–10 g/L. In our experiments, the effect of these two anionic salts (NaCl and Na_2SO_4) on the simultaneous removal of two types of heavy metals was investigated under AER and ANA conditions. All experiments were conducted under the conditions of pH_i = 8.2, j = 60 A/m^2, and $[anions]_0$ 50 = mmol/L.

The final R_{Cd} and R_{Mn} after 40 min AER and ANA processes in single chloride and single sulfate systems are shown in Fig. 7. It is observed that most of Cd^{2+} (around 80%–90%) was eliminated in ANA process regardless of whether chloride or sulfate was added. In AER process, the sulfate system exhibited a more positive effect on Cd^{2+} removal than the chloride system, although both had removal efficiencies of less than 30%. Moreover, the reduction conditions were most conducive to the removal efficiency of Mn^{2+}, followed by the chloride system. Thus, the ranking of the processes with regard to the removal efficiency of Mn^{2+} from high to low was Cl^-–ANA, SO_4^{2-}–ANA, Cl^-–AER, and SO_4^{2-}–AER and the corresponding removal efficiencies were 49.5%, 39.9%, 24.37%, and 15%, respectively. Similar conclusions were reported by many researchers, that is, the positive effect of chloride on heavy metal removal due to the de-passivation of the anode electrode surface [17,47,48].

In brief, the same molar weight (50 mmol/L) of chloride and sulfate has an opposite effect on Cd^{2+} and Mn^{2+} removal. The reason that chloride and sulfate were, respectively, more suitable for Mn^{2+} and Cd^{2+} removal might be attributed to the different approaches and mechanisms for the removal of Cd^{2+} and Mn^{2+}: (1) Cd^{2+} is likely to be removed by adsorption and co-precipitation of hydroxide species. (2) The electroreduction of cathode plays a large role in the removal of Mn^{2+}. (3) The addition of counter ions with higher charges, such as divalent SO_4^{2-} anions, promoted the electric neutralization on the surface of flocs and resulted in rapid settlement [49]. (4) Moreover, charged double layer, adsorption and bridging between particles were enhanced by adding SO_4^{2-} [50]. Thus, the removal efficiency of Cd^{2+} was increased with the addition of SO_4^{2-}.

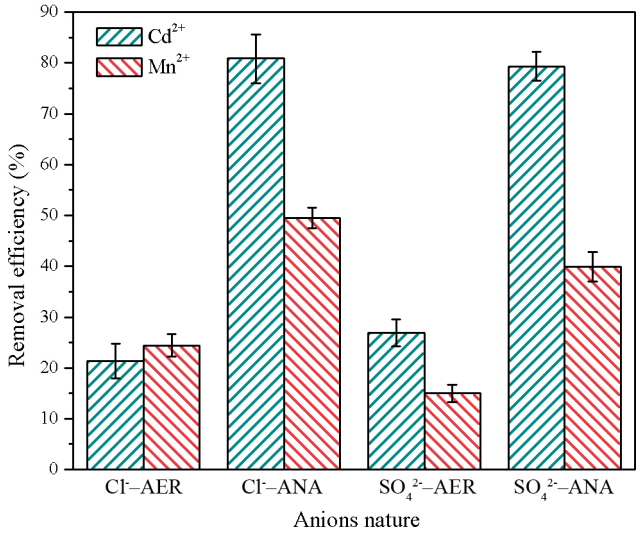

Fig. 7. Effect of Cl^- and SO_4^{2-} ions on Cd^{2+} and Mn^{2+} removal efficiency in AER and ANA processes (pH_i = 8.2, j = 60 A/m^2 and $[anions]_0$ = 50 mmol/L).

3.6. Effect of initial anions concentration

As reported in the literatures [28,37], chloride has a positive effect on the EC process and is generally used as a 'depassivation agent' in industrial applications because it can break down the passivation film generated on the surface of electrodes, whereas sulfate is able to cause the deposition of metal hydroxides/oxyhydroxides. In this study, the effect of the chloride and sulfate concentrations on the heavy metals removal in the AER and ANA processes were investigated. The Cd^{2+} and Mn^{2+} removal efficiencies for the Cl^-–AER, Cl^-–ANA, SO_4^{2-}–AER, and SO_4^{2-}–ANA processes are shown in Figs. 8 and 9, respectively.

The results indicate that both Cd^{2+} and Mn^{2+} are effectively removed in an oxygen-free environment, particularly at low anion concentrations. As an example, more than half of Cd^{2+} was removed in the ANA process (Figs. 8(b) and (d)), whereas the maximum R_{Cd} in the AER process was 43.8% (Fig. 8(c), $[SO_4^{2-}]_0$ = 10 mmol/L). Moreover, R_{Cd} significantly decreased from 31.94% to 11% with increasing $[Cl^-]_0$ from 10 to 200 mmol/L in the AER process. In the ANA process, the concentration of 50 mmol/L Cl^- resulted in the best Cd^{2+} removal efficiency and any increase or decrease in the $[Cl^-]_0$ had an adverse effect on the Cd^{2+} removal. These results are ascribed to the dissolution of the metal hydroxides ($M(OH)_n$) by reacting with Cl^- in a short time [17]. This means that OH^- is displaced by the excess Cl^- and is eventually transformed into soluble $M(OH)_{n-m}Cl_m$ and MCl_{n+1}^- [51]. Figs. 8(c) and (d) show that as $[SO_4^{2-}]_0$ increases from 10 to 50 mmol/L, R_{Cd} decreases from 43.8% to 25% in the AER process, whereas the highest R_{Cd} (97%) was obtained when the SO_4^{2-} concentration was 30 mmol/L in the ANA process. As demonstrated by Huang et al. [47], an inert film quickly formed in a highly concentrated SO_4^{2-} solution and then caused a large decrease in the current efficiency and the Cd^{2+} removal efficiency.

The removal of Mn^{2+} is also affected by the anion concentration. As shown in Figs. 9(a) and (c), in the AER process, less than 30% Mn^{2+} was removed by the chloride and sulfate systems. This efficiency is far below the values achieved in the reduction conditions. In addition, the removal efficiency of Mn^{2+} also decreased with increasing $[Cl^-]_0$ from 10 to 100 mmol/L and $[SO_4^{2-}]_0$ from 10 to 50 mmol/L. However, in the ANA process, regardless of the concentration, the addition of Cl^- hardly affects the removal of Mn^{2+} (46.3%~50.2%) as shown in Fig. 8(c), whereas the R_{Mn} dramatically decreased to 38.96% from 55.1% as the $[SO_4^{2-}]_0$ increased from 10 to 50 mmol/L. Hence, SO_4^{2-}–ANA and Cl^-–ANA are recommended for Cd^{2+} and Mn^{2+} removal, respectively, and the anion concentration should be relatively low.

3.7. Decay kinetics and operational parameters on the reaction rate constant

The removal rate of the metals (Cd and Mn) for different operational parameters (current density, anion type, and concentration) after a 40 min EC process are shown in Tables 2 and 3. The removal rate, namely k (min^{-1}) is

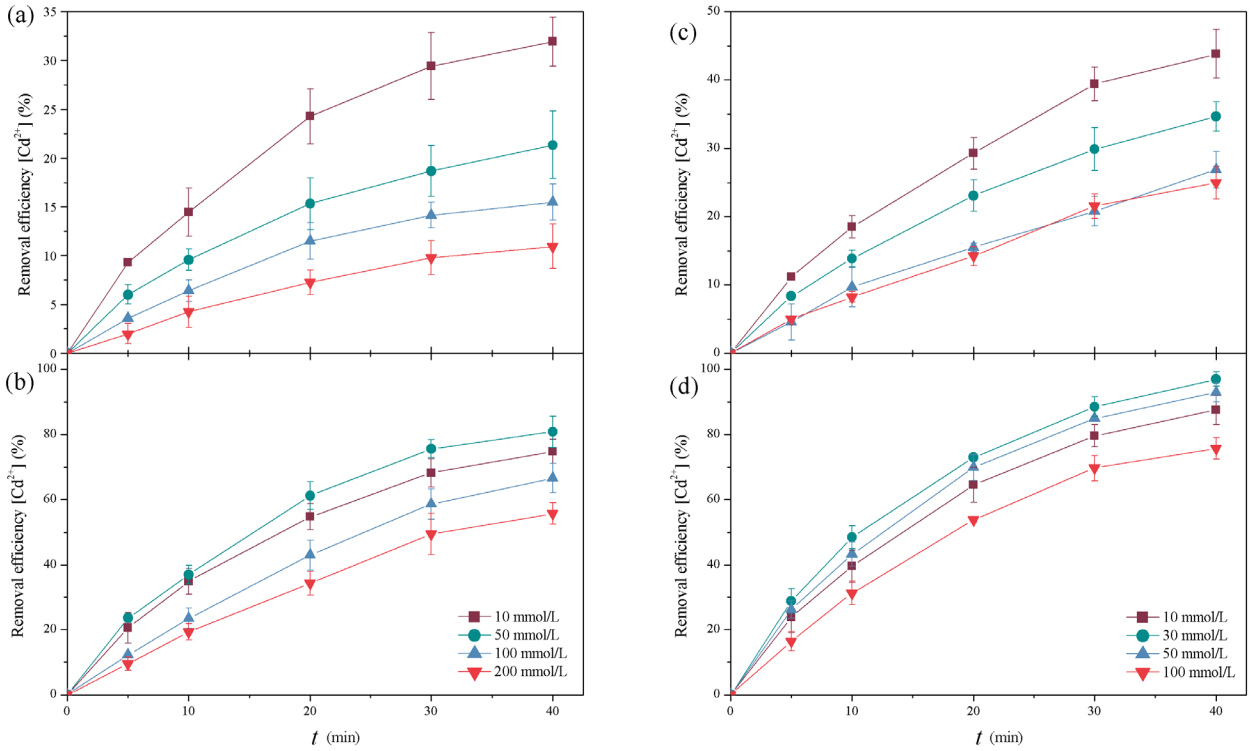

Fig. 8. Effect of $[Cl^-]_0$ and $[SO_4^{2-}]_0$ on Cd^{2+} removal efficiency in AER and ANA processes: (a) Cl^-–AER, (b) Cl^-–ANA, (c) SO_4^{2-}–AER, and (d) SO_4^{2-}–ANA (pH_i = 8.2 and j = 60 A/m^2).

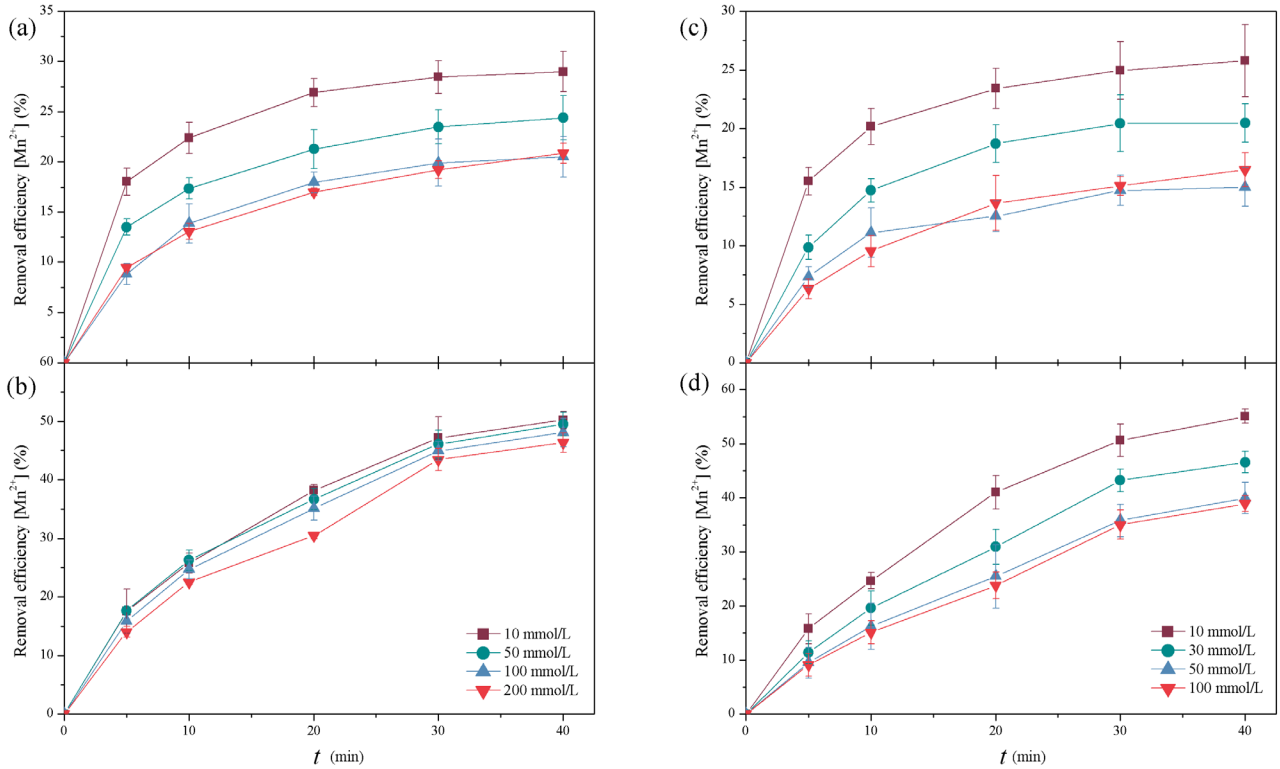

Fig. 9. Effect of $[Cl^-]_0$ and $[SO_4^{2-}]_0$ on Mn^{2+} removal efficiency in AER and ANA processes: (a) Cl^-–AER, (b) Cl^-–ANA, (c) SO_4^{2-}–AER, and (d) SO_4^{2-}–ANA (pH_i = 8.2 and j = 60 A/m^2).

calculated and predicted using a pseudo-first-order model as reported in previous studies [52–55]. The reaction rate constant, '*K*', can be calculated from the plot log [C_t/C_0] vs. reaction time [56,57]. The kinetic parameters and the correlation coefficients (R^2) of the pseudo-first-order model for Cd^{2+} and Mn^{2+} at different current densities are showed in Table 2. The removal of both heavy metals satisfies the pseudo-first-order kinetics adequately (R^2_{min} >0.98). As shown in Table 2, as the current density increased from 20 to 100 A/m^2, the apparent constant of the Cd^{2+} and Mn^{2+} in the AER process did not change much (around k^{app}_{Cd} = 0.03 and k^{app}_{Mn} = 0.11), whereas in the ANA process, the constant increased from k_{Cd} = 0.056 to 0.22 min^{-1} and k_{Mn} = 0.0335 to 0.0777 min^{-1}. The significant improvement in the removal rates of Cd^{2+} with increasing current density in the ANA process is attributed to the generation of the [Fe(II), Fe(III)] layered double hydroxides (i.e., green rust). The removal rate of Cd^{2+} and Mn^{2+} for the different anion types and concentrations also satisfies the pseudo-first-order kinetics (R^2_{min} > 0.983) as shown in Table 3. All of the apparent constants k^{app} decreased with increasing initial chloride and sulfate concentrations for the AER and ANA processes. This result is consistent with the heavy metal removal efficiency shown in Figs. 8 and 9.

Table 2
Predicted parameters of pseudo-first-order removal rates of Cd^{2+} and Mn^{2+} at different current densities (pH_i = 8.2 and $[Cl^-]_0$ = 20 mmol/L)

Items	j (A/m^2)	Pseudo-first order model, $-dC/dt = k^{app}(C-C_e)$			
		k_{Cd} (min^{-1})	R^2	k_{Mn} (min^{-1})	R^2
AER	20	0.0351	0.9917	0.1191	0.9929
	40	0.0302	0.9948	0.1051	0.9823
	60	0.0314	0.9963	0.1094	0.9867
	80	0.0257	0.9986	0.0934	0.9991
	100	0.0321	0.9977	0.1168	0.9969
ANA	20	0.0560	0.9979	0.0335	0.9979
	40	0.0535	0.9995	0.0294	0.9951
	60	0.0675	0.9958	0.0416	0.9991
	80	0.1115	0.9980	0.0445	0.9979
	100	0.2200	0.9978	0.0777	0.9940

In brief, the k^{-app} and the heavy metals removal efficiency improved with increasing current density (ANA) and decreased with increasing NaCl and Na_2SO_4 concentration in the AER and ANA systems after 40 min of reaction time. As reported by Ghernaout et al. [44], cadmium was initially removed by a cathodic reduction followed by coagulation. The removal rate of Cd^{2+} and Mn^{2+} in the AER process exhibited no notable change with the increase in the current density probably because the removal mechanism of Cd^{2+} and Mn^{2+} depended on the cathodic reduction.

In ANA processes, the removal efficiencies of Cd^{2+} and Mn^{2+} were improved with the addition of Na_2SO_4, divalent SO_4^{2-} ions has stronger electric neutralization than monovalent Cl^- ion and promote the flocculation and settling efficiency of Fe flocs (i.e., sulfate GR), larger size of Fe flocs was also observed than single Cl^- solution. The addition of both Cl^- and SO_4^{2-} are working as interlayer anions contributes to the increase in the negative charge of newly formed Fe flocs in the EC process. Refait et al. [58,59] investigated the oxidation of aqueous suspensions of $Fe(OH)_2$ by DO in the presence of sulfate and chloride ions. The results demonstrated that sulfate GR generated instead of chloride green rust even in solutions with large molar ratios of $[Cl^-]/[SO_4^{2-}]$ due to the Fe(II)–Fe(III) LDHs (i.e., GRs) presents stronger affinity for divalent anion (SO_4^{2-}) than univalent anion (Cl^-). Therefore, the removal rates of Cd^{2+} and Mn^{2+} in ANA processes were higher than in AER processes by adsorption and

Table 3
Predicted parameters of pseudo-first order removal rates of Cd^{2+} and Mn^{2+} at different anions concentration (pH_i = 8.2 and j = 60 A/m^2)

Items	$[anions]_0$ mmol/L	Pseudo-first-order model, $-dC/dt = k^{app}(C-C_e)$			
		k_{Cd} (min^{-1})	R^2	k_{Mn} (min^{-1})	R^2
Cl^-–AER	10	0.0546	0.9981	0.1808	0.9917
	50	0.0508	0.9979	0.1476	0.9875
	100	0.0440	0.9973	0.1098	0.9991
	200	0.0318	0.9973	0.1079	0.9881
Cl^-–ANA	10	0.0528	0.99953	0.0659	0.9920
	50	0.0546	0.99782	0.0537	0.9920
	100	0.0295	0.99844	0.0461	0.9966
	200	0.0256	0.99363	0.0517	0.9830
SO_4^{2-}–AER	10	0.0378	0.9989	0.0598	0.9935
	30	0.0412	0.9969	0.0432	0.9992
	50	0.0382	0.9951	0.0521	0.9870
	100	0.0196	0.9948	0.0365	0.9972
SO_4^{2-}–ANA	10	0.0606	0.9993	0.1788	0.9935
	30	0.0513	0.9994	0.1262	0.9992
	50	0.0370	0.9956	0.1332	0.9870
	100	0.4031	0.9978	0.0875	0.9972

co-precipitation of GR hydroxides flocs, particularly in the presence of SO_4^{2-}.

3.8. Isotherm and thermodynamic studies

3.8.1. Isotherm studies

The contaminants (heavy metals) are usually adsorbed by the surface of metallic hydroxides in situ produced during EC process. To investigate the mechanism of the removal process of Cd^{2+} and Mn^{2+}, two adsorption isotherms, that is, Freundlich and Langmuir models were established to evaluate the relationship between the amounts of Cd^{2+} and Mn^{2+} adsorbed onto the Fe hydroxides and its equilibrium concentration in anaerobic and aerobic EC conditions. The Langmuir and Freundlich isotherms are illustrated below [60].

$$\frac{C_e}{q_e} = \frac{1}{K_L Q_{\max}} + \frac{C_e}{Q_{\max}} \tag{15}$$

$$\ln q_e = \ln K_F + b_F \ln C_e \tag{16}$$

where $Q_{\max}$ (mg/g) and K_L (L/mg) are the Langmuir constants, which are corresponding to the capacity of sorption and energy of adsorption, respectively. C_e (mg/L) and q_e (mg/g) are the equilibrium concentration and equilibrium adsorption capacity, respectively [61]. Dimensionless b_F and K_F (L/mg) are constants.

The fitted constants for the two models along with regression coefficients were summarized in Table 4. Of the isotherm models tested, Freundlich model was most appropriate to represent the adsorption/removal equilibrium data of Cd^{2+} and Mn^{2+} under ANA conditions, whereas Langmuir model was appropriate to represent under AER environments, based on the R^2. The calculated values of 'n' in Freundlich model indicates the strength of adsorption and it is desirable if $0 < 1/n < 1$ [62]. Hence, the values of $n > 1$ are favorable for the removal of heavy metals by Fe hydroxides. Based on the values of Q_m calculated by the Langmuir equation, the Cd^{2+} adsorption capacity under ANA condition was about four times higher than that under AER condition, whereas Mn^{2+} adsorption capacity under two conditions was very close to each other. The Langmuir isotherm theory assumes monolayer coverage of adsorbate over a homogenous adsorbent surface. Once an adsorbate molecule occupies a site, no further adsorption can take place at that site [62]. Specifically, it was found that the maximum adsorption capacity for Cd^{2+} and Mn^{2+} under ANA condition were 263.86 and 120.85 mg/g (in iron), and 57.2 and 88.25 mg/g under AER condition, respectively, suggesting heavy metals showed stronger affinity to Fe hydroxides under ANA condition.

3.8.2. Thermodynamic studies

To understand the adsorption thermodynamic performance profoundly, the thermodynamic analysis in the temperature range 288–308 K was conducted to size up the adsorption reaction types (endothermic or exothermic), such as Gibb's free energy change (ΔG, kJ/mol), enthalpy change (ΔH, kJ/mol), and entropy change (ΔS, J/mol·K) were calculated according to the following equations [63]:

$$\ln K = \frac{\Delta S}{R} - \frac{\Delta H}{RT} \tag{17}$$

$$K = \frac{q_e}{C_e} \tag{18}$$

$$\Delta G = \Delta H - T\Delta S \tag{19}$$

where K is the dimensionless equilibrium coefficient (L/mol), R is the gas constant (8.314 J mol^{-1} K^{-1}), and T is the temperature in kelvin.

Table 5 shows the results of thermodynamic studies for Cd^{2+} and Mn^{2+} adsorption under ANA and AER environments. The ΔG values for the temperatures at range of 288–308 K were obtained between –9.8 and –20.15 kJ/mol. Negative values of free energy changes indicated that the adsorption of Cd^{2+} and Mn^{2+} on the Fe hydroxides is a spontaneous and a thermodynamically favorable process. With increasing temperature from 288 to 308 K, the values of ΔG decreased from –17.22 to –20.15 kJ/mol (ANA–Cd), –11.5 to 14.3 kJ/mol (ANA–Mn), –11.5 to –12.5 kJ/mol (AER–Cd), and –9.8 to –10.5 kJ/mol (AER–Mn). The ΔG range –20 ~ 0 kJ/mol represents a physisorption process. Positive values of ΔS indicate the increasing randomness in the adsorption process. The positive values of ΔH suggest the endothermic process. Similar results of Fe hydroxides on heavy metals adsorption were reported by González et al. [64] and Shan et al. [65].

Table 4
Langmuir and Freundlich adsorption isotherm models for Cd^{2+} and Mn^{2+} under ANA and AER environments at 50 mg/L Cd^{2+}, 60 mg/L Mn^{2+}, pH_i = 8.2, j = 20–100 A/m^2, and 298 K

Types	Heavy metals	Langmuir			Freundlich		
		q_m (mg/g)	K_L (L/mg)	R^2	K_F (mg/g)/(L/mg)$^{1/n}$	n	R^2
AER	Cd	57.207	0.237	0.9704	23.365	4.533	0.8342
	Mn	88.248	0.028	0.9863	5.379	1.71	0.9236
ANA	Cd	263.86	0.084	0.9727	29.76	1.706	0.9489
	Mn	120.85	0.304	0.8953	49.706	4.336	0.9773

Table 5
Thermodynamic data for adsorption of Cd^{2+} and Mn^{2+} under ANA and AER environments at 50 mg/L Cd^{2+}, 60 mg/L Mn^{2+}, pH_i = 8.2, j = 60 A/m^2

Type	Heavy metals	Temperature (K)	ΔG (kJ/mol)	ΔH (kJ/mol)	ΔS (J/mol·K)
AER	Cd	288	–11.5	7.22	0.065
		298	–12.1		
		308	–12.5		
	Mn	288	–9.8	5.5	0.053
		298	–10.4		
		308	–10.5		
ANA	Cd	288	–17.22	20.22	0.131
		298	–18.53		
		308	–20.15		
	Mn	288	–11.5	11.5	0.081
		298	–13.1		
		308	–14.3		

4. Conclusions

In this study, a comparison of the AER and ANA processes for the removal of Cd^{2+} and Mn^{2+} from wastewater was conducted and the effects of various operating parameters were investigated. AER and ANA environments are adjusted by Na_2SO_3 and H_2O_2. The following conclusions were drawn:

1. The anaerobic environment is superior to the aerobic environment for the simultaneous removal of Cd^{2+} and Mn^{2+} from wastewater due to the high proportion of Fe(II)/Fe(III) species (green rust) generated in solution; this results in stronger electrostatic absorbability, a larger specific surface area, and better flocculation efficiency.
2. An increase in the removal efficiency of Cd^{2+} and Mn^{2+} is observed with an increase in the current density (j). However, in the AER process, the removal efficiency of Mn^{2+} remains relatively low, even at j = 100 A/m^2 (42.33%), whereas a removal efficiency of 93.83% was obtained in the ANA process.
3. The nature of the anions and the initial concentrations of chloride ($[Cl^-]_0$) and sulfate ($[SO_4^{2-}]_0$) also have a marked effect on both the AER and ANA processes. The observation that chloride is more suitable for Mn^{2+} removal than sulfate ($[anions]_0$ 50 mmol/L) was also reported by previous researchers, whereas sulfate is more suitable for Cd^{2+} removal. However, excess concentrations of chloride or sulfate (>50 mmol/L) have an adverse effect on heavy metal removal in both the AER and ANA processes.
4. The kinetic parameters and the correlation coefficients (R^2) of a pseudo-first-order model of Cd^{2+} and Mn^{2+} at different current densities were investigated. The removal of both heavy metals satisfies the pseudo-first-order kinetics.
5. Isotherm studies were investigated. Freundlich model was most appropriate to represent the adsorption/removal equilibrium data of Cd^{2+} and Mn^{2+} under ANA conditions, whereas Langmuir model was appropriate to represent under AER environments. Thermodynamic studies indicate the adsorption of Cd^{2+} and Mn^{2+} on the Fe hydroxides is a spontaneous and a thermodynamically favorable process.

In conclusion, ANA condition of EC represents an alternative method for cadmium and manganese treatment. The addition of anions should be considered and depends on the heavy metal content.

Acknowledgment

This work was supported by the National Natural Science Foundation of China (Project No. 41562012).

References

[1] N. Colantonio, Y. Kim, Cadmium (II) removal mechanisms in microbial electrolysis cells, J. Hazard. Mater., 311 (2016) 134–141.
[2] E. Gatsios, J.N. Hahladakis, E. Gidarakos, Optimization of electrocoagulation (EC) process for the purification of a real industrial wastewater from toxic metals, J. Environ. Manage., 154 (2015) 117–127.
[3] P. Ganesan, J. Lakshmi, G. Sozhan, S. Vasudevan, Removal of manganese from water by electrocoagulation: adsorption, kinetics and thermodynamic studies, Can. J. Chem. Eng., 91 (2013) 448–458.
[4] S. Vasudevan, J. Lakshmi, M. Packiyam, Electrocoagulation studies on removal of cadmium using magnesium electrode, J. Appl. Electrochem., 40 (2010) 2023–2032.
[5] D. Ghernaout, M.W. Naceur, Ferrate(VI): in situ generation and water treatment – a review, Desal. Wat. Treat., 30 (2011) 319–332.
[6] S. Vasudevan, M.A. Oturan, Electrochemistry: as cause and cure in water pollution—an overview, Environ. Chem. Lett., 12 (2014) 97–108.
[7] R. Kamaraj, P. Ganesan, S. Vasudevan, Use of hydrous titanium dioxide as potential sorbent for the removal of manganese from water, J. Electrochem. Sci. Eng., 4 (2014) 187–201.
[8] S. Vasudevan, J. Lakshmi, Effects of alternating and direct current in electrocoagulation process on the removal of cadmium from water – a novel approach, Sep. Purif. Technol., 80 (2011) 643–651.
[9] A. Sharif, M. Ashraf, A.A. Anjum, A. Javeed, I. Altaf, M.F. Akhtar, M. Abbas, B. Akhtar, A. Saleem, Pharmaceutical wastewater being composite mixture of environmental pollutants may be associated with mutagenicity and genotoxicity, Environ. Sci. Pollut. Res., 23 (2015) 1–8.
[10] B. Wang, Y. Zhu, Z. Bai, R. Luque, J. Xuan, Functionalized chitosan biosorbents with ultra-high performance, mechanical

strength and tunable selectivity for heavy metals in wastewater treatment, Chem. Eng. J., 325 (2017) 350–359.
[11] A.G. El Samrani, B.S. Lartiges, F. Villiéras, Chemical coagulation of combined sewer overflow: heavy metal removal and treatment optimization, Water Res., 42 (2008) 951–960.
[12] N. Drouiche, M.W. Naceur, H. Boutoumi, N. Aitmessaoudene, R. Henniche, T. Ouslimane, Assessment of the recovery of photovoltaic cells cutting fluid by chemical pretreatment and ultrafiltration, Desal. Wat. Treat., 51 (2013) 713–716.
[13] Q. Zhu, Z. Li, Hydrogel-supported nanosized hydrous manganese dioxide: synthesis, characterization, and adsorption behavior study for Pb^{2+}, Cu^{2+}, Cd^{2+} and Ni^{2+} removal from water, Chem. Eng. J., 281 (2015) 69–80.
[14] A. Dabrowski, Z. Hubicki, P. Podkoscielny, E. Robens, Selective removal of the heavy metal ions from waters and industrial wastewaters by ion-exchange method, Chemosphere, 56 (2004) 91–106.
[15] T.A. Kurniawan, G.Y.S. Chan, W.H. Lo, S. Babel, Physico–chemical treatment techniques for wastewater laden with heavy metals, Chem. Eng. J., 118 (2006) 83–98.
[16] L. Semerjian, A. Damaj, D. Salam, Comparative study of humic acid removal and floc characteristics by electrocoagulation and chemical coagulation, Environ. Monit. Assess., 187 (2015) 670.
[17] S. Aoudj, A. Khelifa, N. Drouiche, R. Belkada, D. Miroud, Simultaneous removal of chromium(VI) and fluoride by electrocoagulation–electroflotation: application of a hybrid Fe-Al anode, Chem. Eng. J., 267 (2015) 153–162.
[18] D. Ghernaout, M.W. Naceur, B. Ghernaout, A review of electrocoagulation as a promising coagulation process for improved organic and inorganic matters removal by electrophoresis and electroflotation, Desal. Wat. Treat., 28 (2011) 287–320.
[19] J. Lu, Y. Li, M. Yin, X. Ma, S. Lin, Removing heavy metal ions with continuous aluminum electrocoagulation: a study on back mixing and utilization rate of electro-generated Al ions, Chem. Eng. J., 267 (2015) 86–92.
[20] G. Mouedhen, M. Feki, P. Wery Mde, H.F. Ayedi, Behavior of aluminum electrodes in electrocoagulation process, J. Hazard. Mater., 150 (2008) 124–135.
[21] M. Kobya, U. Gebologlu, F. Ulu, S. Oncel, E. Demirbas, Removal of arsenic from drinking water by the electrocoagulation using Fe and Al electrodes, Electrochim. Acta, 56 (2011) 5060–5070.
[22] S. Irki, D. Ghernaout, M.W. Naceur, Decolourization of Methyl Orange (MO) by electrocoagulation (EC) using iron electrodes under a magnetic field (MF), Desal. Wat. Treat., 79 (2017) 368–377.
[23] D. Ghernaout, B. Ghernaout, A. Boucherit, M.W. Naceur, A. Khelifa, A. Kellila, Study on mechanism of electrocoagulation with iron electrodes in idealised conditions and electrocoagulation of humic acids solution in batch using aluminium electrodes, Desal. Wat. Treat., 8 (2009) 91–99.
[24] D. Ghernaout, Advanced oxidation phenomena in electrocoagulation process: a myth or a reality?, Desal. Wat. Treat., 51 (2013) 7536–7554.
[25] D. Cao, H. Zeng, B. Yang, X. Zhao, Mn assisted electrochemical generation of two-dimensional Fe-Mn layered double hydroxides for efficient Sb(V) removal, J. Hazard. Mater., 336 (2017) 33–40.
[26] M. Kobya, E. Gengec, E. Demirbas, Operating parameters and costs assessments of a real dyehouse wastewater effluent treated by a continuous electrocoagulation process, Chem. Eng. Process., 101 (2016) 87–100.
[27] C. Delaire, C.M. van Genuchten, S.E. Amrose, A.J. Gadgil, Bacteria attenuation by iron electrocoagulation governed by interactions between bacterial phosphate groups and Fe(III) precipitates, Water Res., 103 (2016) 74–82.
[28] U. Tezcan Un, S.E. Onpeker, E. Ozel, The treatment of chromium containing wastewater using electrocoagulation and the production of ceramic pigments from the resulting sludge, J. Environ. Manage., 200 (2017) 196–203.
[29] M. Kobya, A. Akyol, E. Demirbas, M.S. Oncel, Removal of arsenic from drinking water by batch and continuous electrocoagulation processes using hybrid Al-Fe plate electrodes, Environ. Prog. Sustain., 33 (2014) 131–140.
[30] W. Wan, T.J. Pepping, T. Banerji, S. Chaudhari, D.E. Giammar, Effects of water chemistry on arsenic removal from drinking water by electrocoagulation, Water Res., 45 (2011) 384–392.
[31] K.L. Dubrawski, M. Mohseni, In-situ identification of iron electrocoagulation speciation and application for natural organic matter (NOM) removal, Water Res., 47 (2013) 5371–5380.
[32] S.V. Jadhav, E. Bringas, G.D. Yadav, V.K. Rathod, I. Ortiz, K.V. Marathe, Arsenic and fluoride contaminated groundwaters: a review of current technologies for contaminants removal, J. Environ. Manage., 162 (2015) 306–325.
[33] R. Li, C. He, Y. He, Preparation and characterization of poly-silicic-cation coagulant from industrial wastes, Desalination, 319 (2013) 85–91.
[34] I. Heidmann, W. Calmano, Removal of Cr(VI) from model wastewaters by electrocoagulation with Fe electrodes, Sep. Purif. Technol., 61 (2008) 15–21.
[35] C.M. van Genuchten, J. Peña, S.E. Amrose, A.J. Gadgil, Structure of Fe(III) precipitates generated by the electrolytic dissolution of Fe(0) in the presence of groundwater ions, Geochim. Cosmochim. Acta, 127 (2014) 285–304.
[36] E. Bazrafshan, A.H. Mahvi, S. Nasseri, A.R. Mesdaghinia, F. Vaezi, S. Nazmara, Removal of cadmium from industrial effluents by electrocoagulation process using iron electrodes, Iran. J. Environ. Health, (2006) 261–266.
[37] P. Song, Z. Yang, G. Zeng, X. Yang, H. Xu, L. Wang, R. Xu, W. Xiong, K. Ahmad, Electrocoagulation treatment of arsenic in wastewaters: a comprehensive review, Chem. Eng. J., 317 (2017) 707–725.
[38] K.L. Dubrawski, C.M. van Genuchten, C. Delaire, S.E. Amrose, A.J. Gadgil, M. Mohseni, Production and transformation of mixed-valent nanoparticles generated by Fe(0) electrocoagulation, Environ. Sci. Technol., 49 (2015) 2171.
[39] N. Ardhan, E.J. Moore, C. Phalakornkule, Novel anode made of iron scrap for a reduced-cost electrocoagulator, Chem. Eng. J., 253 (2014) 448–455.
[40] M. Al-Shannag, Z. Al-Qodah, K. Bani-Melhem, M.R. Qtaishat, M. Alkasrawi, Heavy metal ions removal from metal plating wastewater using electrocoagulation: kinetic study and process performance, Chem. Eng. J., 260 (2015) 749–756.
[41] C. Hu, S. Wang, J. Sun, H. Liu, J. Qu, An effective method for improving electrocoagulation process: optimization of Al13 polymer formation, Colloids Surf. A, 489 (2016) 234–240.
[42] A. Guzman, J.L. Nava, O. Coreno, I. Rodriguez, S. Gutierrez, Arsenic and fluoride removal from groundwater by electrocoagulation using a continuous filter-press reactor, Chemosphere, 144 (2016) 2113–2120.
[43] V. Khandegar, A.K. Saroha, Electrocoagulation for the treatment of textile industry effluent--a review, J. Environ. Manage., 128 (2013) 949–963.
[44] D. Ghernaout, M.W. Naceur, A. Aouabed, On the dependence of chlorine by-products generated species formation of the electrode material and applied charge during electrochemical water treatment, Desalination, 270 (2011) 9–22.
[45] C.A. Martínez-Huitle, E. Brillas, Decontamination of wastewaters containing synthetic organic dyes by electrochemical methods: a general review, Appl. Catal., B, 87 (2009) 105–145.
[46] K. Cheballah, A. Sahmoune, K. Messaoudi, N. Drouiche, H. Lounici, Simultaneous removal of hexavalent chromium and COD from industrial wastewater by bipolar electrocoagulation, Chem. Eng. Process., 96 (2015) 94–99.
[47] C.-H. Huang, L. Chen, C.-L. Yang, Effect of anions on electrochemical coagulation for cadmium removal, Sep. Purif. Technol., 65 (2009) 137–146.
[48] L. Xu, Q. Huang, X. Xu, G. Cao, C. He, Y. Wang, M. Yang, Simultaneous removal of Zn^{2+} and Mn^{2+} ions from synthetic and real smelting wastewater using electrocoagulation process: influence of pulse current parameters and anions, Sep. Purif. Technol., 188 (2017) 316–328.
[49] D. Ghernaout, B. Ghernaout, On the controversial effect of sodium sulphate as supporting electrolyte on electrocoagulation process: a review, Desal. Wat. Treat., 27 (2011) 243–254.
[50] D. Ghernaout, S. Irki, A. Boucherit, Removal of Cu^{2+} and Cd^{2+}, and humic acid and phenol by electrocoagulation using iron electrodes, Desal. Wat. Treat., 52 (2013) 3256–3270.

[51] S.I. Pyun, S.M. Moon, S.H. Ahn, S.S. Kim, Effects of Cl^-, NO^-_3 and SO^{2-}_4 ions on anodic dissolution of pure aluminum in alkaline solution, Corros. Sci., 41 (1999) 653–667.
[52] L. Rajic, N. Fallahpour, E. Podlaha, A. Alshawabkeh, The influence of cathode material on electrochemical degradation of trichloroethylene in aqueous solution, Chemosphere, 147 (2016) 98–104.
[53] D.G. Bassyouni, H.A. Hamad, E.Z. El-Ashtoukhy, N.K. Amin, M.M.A. El-Latif, Comparative performance of anodic oxidation and electrocoagulation as clean processes for electrocatalytic degradation of diazo dye Acid Brown 14 in aqueous medium, J. Hazard. Mater., 335 (2017) 178–187.
[54] R. Kamaraj, P. Ganesan, S. Vasudevan, Removal of lead from aqueous solutions by electrocoagulation: isotherm, kinetics and thermodynamic studies, Int. J. Electrochem. Sci., 12 (2015) 683–692.
[55] P. Ganesan, R. Kamaraj, G. Sozhan, S. Vasudevan, Oxidized multiwalled carbon nanotubes as adsorbent for the removal of manganese from aqueous solution, Environ. Sci. Pollut. Res., 20 (2013) 987–996.
[56] S. Vasudevan, J. Lakshmi, Electrochemical removal of boron from water: adsorption and thermodynamic studies, Can. J. Chem. Eng., 90 (2012) 1017–1026.
[57] A. Shafaei, M. Rezaie, M. Nikazar, Evaluation of Mn^{2+} and Co^{2+} removal by electrocoagulation: a case study, Chem. Eng. J., 50 (2011) 1115–1121.
[58] P. Refait, J.B. Memet, C. Bon, R. Sabot, J.M.R. Génin, Formation of the Fe(II)–Fe(III) hydroxysulphate green rust during marine corrosion of steel, Corros. Sci., 45 (2003) 833–845.
[59] P. Refait, M. Abdelmoula, J.M.R. Génin, R. Sabot, Green rusts in electrochemical and microbially influenced corrosion of steel, C. R. Geosci., 338 (2006) 476–487.
[60] S.M. Wabaidur, M.A. Khan, M.R. Siddiqui, Z.A. Alothman, S. Vasudevan, M.S. Al-Gamdi, I.H. Al-Sohami, Dodecyl sulfate chain anchored bio-char to sequester triaryl methane dyes: equilibrium, kinetics, and adsorption mechanism, Desal. Wat. Treat., 67 (2017) 357–370.
[61] S. Vasudevan, J. Lakshmi, Process conditions and kinetics for the removal of copper from water by electrocoagulation, Environ. Eng. Sci., 29 (2012) 563–572.
[62] J. Hong, Z. Zhu, H. Lu, Y. Qiu, Synthesis and arsenic adsorption performances of ferric-based layered double hydroxide with α-alanine intercalation, Chem. Eng. J., 252 (2014) 267–274.
[63] R. Kamaraj, A. Pandiarajan, S. Jayakiruba, M. Naushad, S. Vasudevan, Kinetics, thermodynamics and isotherm modeling for removal of nitrate from liquids by facile one-pot electrosynthesized nano zinc hydroxide, J. Mol. Liq., 215 (2016) 204–211.
[64] M.A. González, I. Pavlovic, C. Barriga, Cu(II), Pb(II) and Cd(II) sorption on different layered double hydroxides. A kinetic and thermodynamic study and competing factors, Chem. Eng. J., 269 (2015) 221–228.
[65] R.R. Shan, L.G. Yan, K. Yang, Y.F. Hao, B. Du, Adsorption of Cd(II) by Mg-Al-CO_3- and magnetic Fe_3O_4/Mg-Al-CO_3-layered double hydroxides: kinetic, isothermal, thermodynamic and mechanistic studies, J. Hazard. Mater., 299 (2015) 42–49.